Geophysical characterization and monitoring of subsurface drip irrigation, Powder River Basin, Wyoming, USA

*Burke J. Minsley
U.S. Geological Survey
Denever, Colorado, USA
bminsley@usgs.gov

Bruce D. Smith
U.S. Geological Survey
Denver, Colorado, USA
bsmith@usgs.gov

Richard Hammack
National Energy Technology Laboratory
Pittsburgh, Pennsylvania, USA
Richard.Hammack@netl.doe.gov

James I. Sams
National Energy Technology Laboratory
Pittsburgh, Pennsylvania, USA
James.Sams@netl.doe.gov

Garret Veloski
National Energy Technology Laboratory
Pittsburgh, Pennsylvania, USA
Garret.Veloski@netl.doe.gpv

SUMMARY

Water that has been co-produced with coal bed methane in the Powder River Basin, Wyoming, is being applied to agricultural fields using subsurface drip irrigation (SDI). Ground-based frequency-domain electromagnetic (EM) data are acquired over several fields in order to monitor changes in subsurface electrical properties related to the SDI operations. These data indicate spatial variability in soil properties across the site, as well as a systematic increase in conductivity in one field observed on three repeat surveys carried out over one year.

A quantitative assessment of changes in subsurface properties requires inversion of the EM data to recover the true distribution of electrical resistivity with depth. Data calibration and filtering procedures are presented that correct for systematic and random errors in the data, which results in improved inversion estimates.

Key words: electromagnetic, subsurface drip irrigation, monitoring, inversion

INTRODUCTION

Subsurface drip irrigation (SDI) has recently been implemented as a means for beneficially disposing of water co-produced with coal bed methane in the Powder River Basin (PRB), Wyoming (Engle et al., 2009). Because of the sodic and moderately saline nature of the PRB water, careful application is needed in order to prevent damage to the near-surface soil structure or salinization of the soils and deeper groundwater system. The National Energy Technology Laboratory and the U.S. Geological Survey are collaborating with BeneTerra LLC to comprehensively monitor an SDI system using geophysical and geochemical methods.

Repeat electromagnetic (EM) geophysical surveys have been carried out at the Headgate Draw SDI site (figure 1) to characterize baseline conditions and monitor changes in subsurface properties over time (Sams et al., 2008). The GEM-2[1], a multi-frequency electromagnetic instrument that is primarily sensitive to the subsurface electrical conductivity

---

[1] Any use of trade, product, or firm names is for descriptive purposes only and does not imply endorsement by the U.S. Government

structure, was towed along 20 m-spaced survey lines over multiple irrigation fields covering approximately 1.2 km^2.
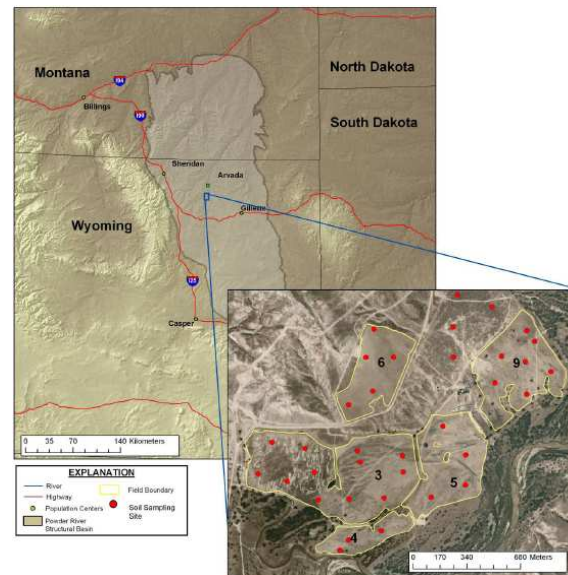
Figure 1. Location of the Headgate Draw project study area within the Powder River Basin, Wyoming. Inset shows numbered agricultural fields.

The EM geophysical data can be utilized to help monitor the fate of the SDI water because changes in subsurface electrical conductivity (EC) can be attributed to changes in saturation and/or salinity. Properly quantifying these subsurface changes in terms of meaningful EC values and their spatiotemporal distribution requires survey procedures and data processing strategies that reduce systematic instrument errors (drift and calibration and calibration) as well as random noise.

We present strategies for filtering, calibrating, and inverting the multi-frequency EM data that are specifically designed to preserve important spectral relationships within the data that are lost when using traditional processing methods. The data collection and processing methods presented here result in frequency domain electromagnetic data that are inverted to recover models that can be quantitatively interpreted both in time and space.

ELECTROMAGNETIC SURVEYS

Six EM surveys have been acquired over the study area, beginning with a pre-SDI installation survey in June 2007.

The surveys were acquired using the GEM-2 instrument mounted on a sled constructed of PVC pipe. The sled was towed behind a utility vehicle equipped with a differential GPS navigation system used for both real-time navigation and recording position information. Data were acquired at five frequencies (1530 Hz, 8250 Hz, 23070 Hz, 33030 Hz, and 47970 Hz) at a sampling rate of 10 Hz and 25 m line spacing.

Figure 2 shows an apparent conductivity map generated from the 47970 Hz data collected in August 2009. Variability in apparent conductivity values across the site can be attributed to depositional changes such as grain size or clay fraction, as well as SDI-induced changes in saturation and/or salinity. In general, non-irrigated areas outside the pink boxes tend to have lower conductivity.
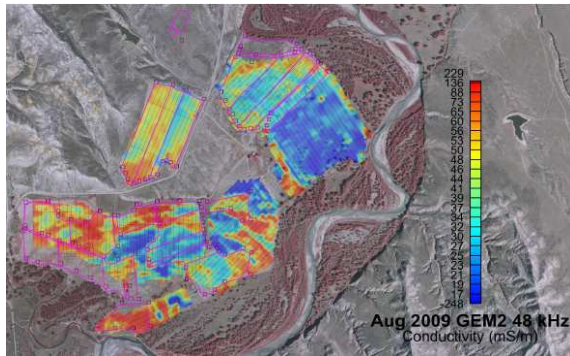
Figure 2. Apparent conductivity map generated using the 48 kHz data for five fields surveyed with the GEM-2 in August 2009. Black lines are survey tracks, and pink lines outline active subsurface drip irrigation areas.

Figure 3 shows snapshots of the apparent conductivity calculated from the 48 kHz data over field 6 between October 2008 (SDI system installed, but not operating) and August 2009 (SDI system in operation). A systematic increase in conductivity is observed over this period, which is likely associated with the SDI operation, though further research is needed to identify whether this trend is associated with increased saturation and dissolution of salts in the vadose zone, increases in salinity due to the SDI, or some combination of these (Engle et al., 2009).
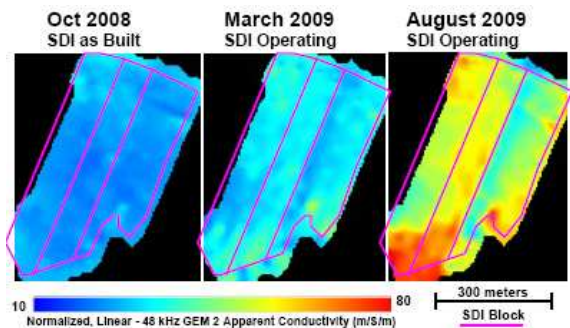
Figure 3. Temporal changes in apparent conductivity at 48 kHz for field 6 at the Headgate Draw site. The pink lines indicate blocks of the SDI system where the drip lines are laid out parallel to the long axis

DATA PROCESSING AND INVERSION

While time-lapse apparent conductivity maps are very useful in assessing semi-quantitative changes in conductivity at the site, we also focus on a more rigorous analysis of the data to better quantify conductivity values and their distribution with depth. Recovering true conductivity profiles as a function of depth requires inversion of the EM data. In this work, we use the one-dimensional (1D) frequency domain inversion code, em1dfm (Farquharson et al., 2003).

Before inversion, it is important to remove both systematic and random errors from the data. Here, we implement a calibration strategy, originally introduced for airborne EM surveys (Deszcz-Pan et al., 1998), that utilizes a direct current resistivity survey to correct for systematic errors in the EM data. Additionally, we introduce a physically-based filtering method that removes random errors from the EM data.

Calibration

The calibration method developed by Deszcz-Pan *et al.* (1998) for airborne datasets corrects for errors in instrument gain, phase, and bias. This method results in both multiplicative and additive calibration terms, shown in equation (1), where each term is implicitly a function of frequency.

$$d_{obs}^I + jd_{obs}^Q = Ge^{j\phi}\left(d_{cal}^I + jd_{cal}^Q + B^I + jB^Q\right) \qquad (1)$$

The observed data, d_{obs}^I and d_{obs}^Q, are the in-phase and quadrature response in ppm, and $j = \sqrt{-1}$. d_{cal}^I and d_{cal}^Q represent the theoretical in-phase and quadrature response predicted for a known earth model that is spatially coincident with the observed FDEM data, and are computed using the forward modeling algorithm em1dfmfwd (Farquharson *et al.*, 2003). For each frequency, the calibration parameters include a gain factor (G), a phase (ϕ), and in-phase and quadrature bias terms (B^I and B^Q), which are determined using a nonlinear least-squares algorithm that minimizes the difference between the left and right sides of equation (1).

Filtering

We present a new approach to filtering EM data that, like spatial filtering, reduces random noise in the data, but also has several important properties: (1) it is based on the fact that the data at different frequencies are correlated (which is often cited as a drawback to this kind of data), (2) it operates on all of the data simultaneously, thereby preserving important spectral relationships within the data, and (3) it does not involve the imposition of an arbitrary filter smoothing length.

This approach utilizes principal component analysis (PCA) filtering of the data, which, by definition, preserves the component of the data that is most highly correlated across frequencies. The PCA filter is based on the singular value decomposition of the data matrix, **D**, which contains all of the data for a single survey line and has *nf* (number of frequency) rows, and *ns* (number of soundings) columns, where each element in the matrix is a complex number composed of the in-phase and quadrature components of the data.

$$\mathbf{D} = \mathbf{USV}^T \qquad (2)$$

Filtering is accomplished by reconstructing **D** from only *k* of the singular values and singular vectors, where *k* < *nf*. This is equivalent to operating on the original data matrix with a filter constructed from *k* left singular vectors, as shown in equation (3).

$$\mathbf{D}_{filt} = \mathbf{U}_k \mathbf{S}_k \mathbf{V}_k^T = \mathbf{U}_k \mathbf{U}_k^T \mathbf{D} \qquad (3)$$

Calibration and filtering example

A two-dimensional (2D) direct current (DC) resistivity profile was acquired along approximately 200 m of line surveyed with the GEM-2 in field 3 at the Headgate Draw site. The resistivity model resulting from the inversion of this data (figure 4A) is used as the "known" earth model for the calibration procedure. Synthetic EM data are found by computing the forward response to this model, and the calibration parameters that best fit the entire line of data are computed according to equation (1). After calibration, the data are filtered using the PCA approach described above, and are then inverted.

Figure 5 illustrates data at a single frequency (3930 Hz) for the various stages of calibration and filtering. In-phase and quadrature data are shown in (A) and (B), respectively. The phase-amplitude relationship in the data is shown in (C); preserving the correct phase-amplitude relationship across frequencies is a critical step in obtaining good inversion results.

There are two important differences between the data predicted from the DC resistivity model (black) and the measured GEM-2 data (solid green dots): (1) a shift in magnitude and offset in phase-amplitude space due to calibration errors and (2) scatter in the GEM-2 data due to random noise. After calibration (open green circles), the measured data are much better aligned with the data predicted from the calibration model, but still exhibit scatter due to random noise. The inverted calibration factors for this frequency are $G = 0.94$, $\phi = -4.2°$, $B^I = -294$, and $B^Q = 89$. Finally, application of the PCA filter to the calibrated data results in the data shown by orange crosses. The calibrated and filtered data now closely match the character of the data predicted from the DC resistivity model.

The benefit of calibration and filtering on the inversion of the EM data is shown in (figure 4B – D). Figure 4B illustrates the result of inverting the raw GEM-2 data. Although the general trends in the near-surface are captured, the inversion results suggest increased resistivity values at depth, which is in disagreement with the DC resistivity model. Figure 4C shows the result of applying a traditional spatial smoothing filter to the data before inversion. The filtering process has removed some of the jitter due to random noise, but the resulting model still suggests increased resistivity at depth. Finally, figure 4D illustrates the inversion results that incorporate the calibrated and PCA-filtered data. This final model reflects the lower resistivity at depth found from the DC resistivity survey.

To quantify the improvements found by calibrating and filtering the GEM-2 data, Table 1 summarizes the data misfit found during inversion as well as the difference between the inverted resistivity models and the DC resistivity model for the cases in (Figure 4B – D). The model difference is quantified as the norm between models, i.e. $\left\| m^{inverted} - m^{DC} \right\|^2$.

Table 1. Summary of inversion data misfit and proximity to the DC resistivity model for the GEM-2 inversions in (Figure 4B – D).

	Inversion data misfit	Norm of difference between inverted model and DC resistivity model
Raw GEM-2 data (Figure 4B)	67	1005
Smoothed GEM-2 data (Figure 4C)	44	960
Calibrated and filtered GEM-2 data (Figure 4D)	3	229

Table 1 highlights a very important fact: the inversion data misfit using the calibrated and filtered data is significantly improved. Without calibration, it is not possible to recover resistivity models that agree with the data due to systematic errors in the data. This lends significant confidence to the model shown in Figure 4D compared with the other results. Additionally, the model in Figure 4D agrees much more closely with the DC resistivity model, as quantified by the model difference norm.

While this calibration procedure can be valuable in recovering meaningful resistivity models, it is important to note that the result is only as good as the model used for calibration (the DC resistivity profile in this case). The choice of a calibration model should therefore be made carefully.

CONCLUSIONS

Monitoring the effect of SDI operations on groundwater and soil properties is an important task at the Headgate Draw field site. EM surveys that detect changes in subsurface electrical properties are an effective means for accomplishing this task because these data are sensitive to changes in saturation and salinity. In order to more accurately assess changes in the subsurface, we focus on calibration and filtering strategies for the EM data that correct for both systematic and random errors. Inversion of this processed data leads to models of subsurface properties that can be used to more reliably quantify changes due to the SDI operation.

REFERENCES

Deszcz-Pan, M., Fitterman, D.V. and Labson, V.F., 1998. Reduction of inversion errors in helicopter EM data using auxiliary information. Exploration Geophysics, 29: 142-146.

Engle, M.A., Bern, C.R., Healy, R.W., Sams, J.I., Zupancic, J. and Schroeder, K., 2009. Subsurface drip irrigation as a method to beneficially use coalbed methane produced water: Initial impacts to groundwater, soil water, and surface water. Geological Society of America Abstracts with Programs, 41(7).

Farquharson, C.G., Oldenburg, D.W. and Routh, P.S., 2003. Simultaneous 1D inversion of loop--loop electromagnetic data for magnetic susceptibility and electrical conductivity. Geophysics, 68(6): 1857-1869.

Sams, J.I., Lipinski, B.A. and Veloski, G., 2008. Using ground based geophysics to evaluate hydrogeologic effects of

subsurface drip irrigation systems used to manage produced water in the Powder River Basin, Wyoming. Symposium on

the Application of Geophysics to Engineering and Environmental Problems, 21(1): 916-925.
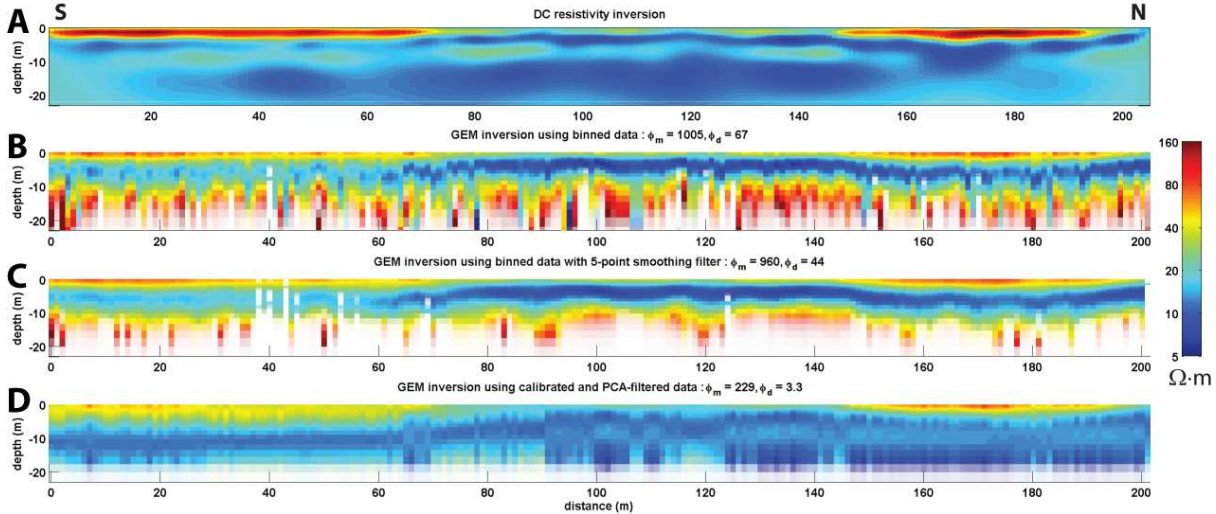
Figure 4. (A) Resistivity model resulting from the inversion of a 2D DC resistivity dataset. (B) Inversion of raw GEM-2 data collected along the same transect as the DC resistivity profile in A. (C) Inversion of GEM-2 data that have been smoothed with a spatial averaging filter. (D) Inversion of GEM-2 data that have been calibrated using the DC resistivity profile and filtered using the PCA approach.
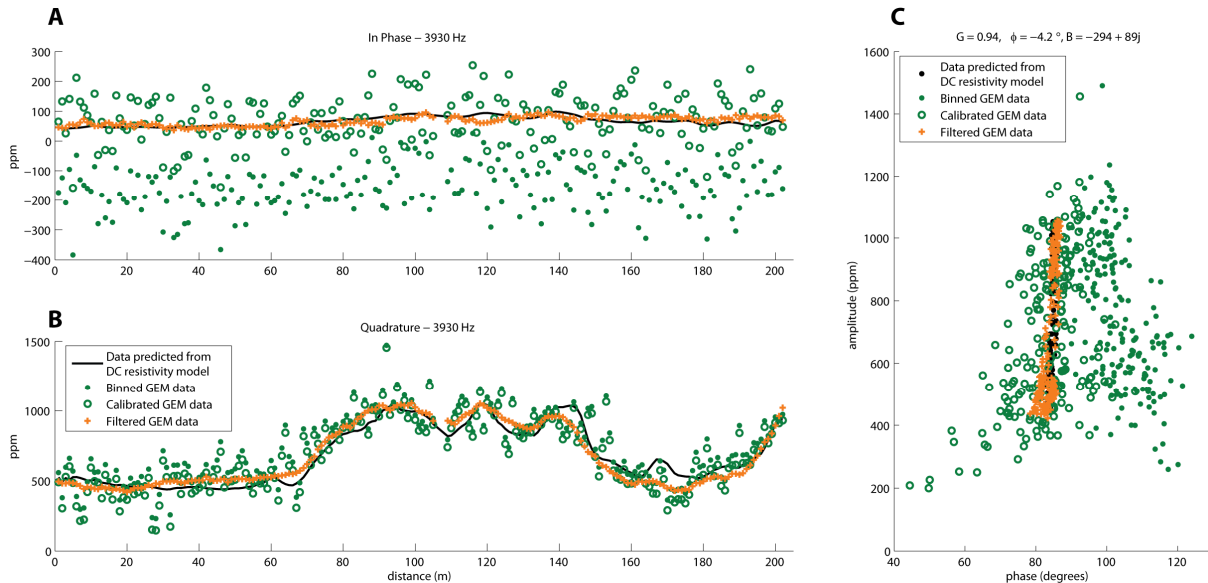
Figure 5. (A) In-phase and (B) quadrature data for various stages of the calibration and filtering process for a single frequency (3930 Hz). The phase-amplitude relationship of these data are illustrated in (C). Data predicted from the DC resistivity model are shown in black, measured GEM-2 data are shown as solid green dots, calibrated GEM-2 data are open green circles, and calibrated and filtered GEM-2 data are orange crosses.